JACS
JOURNAL OF THE AMERICAN CHEMICAL SOCIETY
pubs.acs.org/JACS
Article

Tuning the Properties of Hydrazone/Isosorbide-Based Switchable Chiral Dopants

Brandon Balamut, Russell P. Hughes, and Ivan Aprahamian*

Cite This: J. Am. Chem. Soc. 2024, 146, 24561−24569
Read Online
ACCESS | Metrics & More | Article Recommendations | Supporting Information

ABSTRACT: The long-range supramolecular interactions in liquid crystals (LCs) can be used to amplify and subsequently propagate microscopic structural changes into macroscopic events. Here, we report on a systematic structure−property analysis using 16 chiral photoswitchable dopants composed of bistable hydrazones and chiral isosorbide moieties. Our findings showcase the relationship between the dopant's structure and its helical twisting power (β), and hence, the photophysical properties of the host LC. We show that an increase in the hydrazone CNNH dihedral angle results in an increase in the β value, while alkoxy chains do not lead to such an increase. These results contradict established rules of thumb, stating that structural rigidity and long alky chains are needed for high β values. We also found that the position of the substitution, whether at the 2′ or 5′ positions of the isosorbide unit, or the attachment of the chiral unit to the rotor or stator phenyl units can have negative or positive additive effects that can either increase or decrease the β values. These results made us hypothesize that unsymmetrically functionalized dopants should result in large $\Delta\beta$ values, which we corroborated experimentally. Moreover, a fluorine-functionalized dopant resulted in higher overall β values, most likely because of $\pi-\pi$ interactions. Finally, the dopants were used in modulating and locking in the reflective properties of LC films, yielding multicolor LC canvases that can reflect light from the ultraviolet to the infrared range (i.e., a manipulation of up to ca. 1500 nm of reflected light).

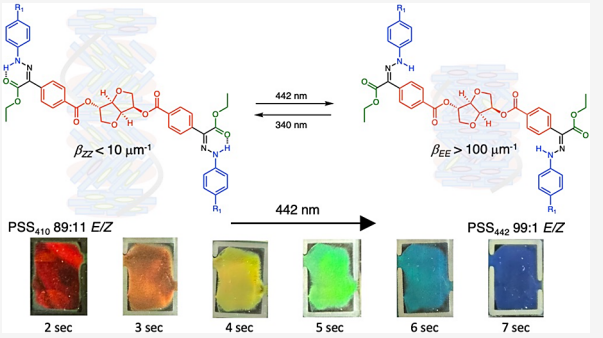

INTRODUCTION

Adaptive liquid crystals (LCs) are of interest to the scientific community because of the wide range of applications they can give rise to, ranging from sensors to smart surfaces, color filters, and beam steerers.[1] These applications usually rely on the introduction of stimuli-responsive chiral dopants to nematic mesogens, which in turn convert them to cholesteric liquid crystals (CLCs) having a helical self-organization.[2] The modulation of the structure of the adaptive dopant consequently alters the noncovalent supramolecular interactions in the LC resulting in changes in the selective reflectance along the helical director of the LC. The thus produced structural color, unlike the color we observe through absorption transitions, results from the diffraction and interference anisotropy that light experiences when passing through the microscopically packed helical assembly.[3] Aside from using thermal,[4] chemical,[5] and electrical[6] stimuli to affect the structural changes in the dopants, light-control, through the use of photochromic chiral dopants, has emerged as a desirable conduit because it affords noninvasive adaptation with high spatial and temporal resolution.[7] Several molecular photoswitches (i.e., azobenzenes, overcrowded alkenes, diarylethenes (DAs), spirooxazines, and fulgides)[2f] have been used in such applications, with azobenzene leading the pack.[8] In general, though, chiral dopants based on this photochromic unit result in transient self-assembled LCs, i.e., the photophysical properties cannot be maintained over time. To address this limitation, bistable DA switches have been used as chiral dopants, resulting in a limited number of systems in which the LC self-assemblies can be locked in place.[9] In general, the use of DA however, results in low helical twisting power (β) and change in the power ($\Delta\beta$) and is fraught with synthetic difficulties and other challenges (e.g., photodegradation[10]).

Another important obstacle in the field is the lack of guiding principles that can explain how the molecular structure of the dopant determines the β and $\Delta\beta$ values.[11] In general, the larger these values, the larger the window of wavelengths that can be reflected, using a minimal amount of doping.[12] However, designing new dopants that satisfy these criteria is usually an empirical walk in the dark with limited guiding hypotheses. The consensus in the literature is that a rigid chiral conformation is needed to obtain high β values. It is hypothesized that such rigid conformations yield optimal

Received: June 10, 2024
Revised: August 9, 2024
Accepted: August 12, 2024
Published: August 20, 2024

$\pi-\pi$ interactions and, hence, chirality transfer between the chiral dopant and mesogen; however, the fine details of how this transfer occurs are unclear. For example, while binaphthyl-based dopants result in one of the highest measured β values (757 μm^{-1}) for switchable chiral dopants, the structurally related biphenyl-based ones only yield low to medium range β values.[13] Similar disconnects can also be found when multiple chiral units are attached to a central switch; while the effect might be additive in β values, it might not be the case for $\Delta\beta$ values, or vice versa.[14] Addressing this disparity is compounded by the fact that traditional single switch dopants are structurally limited in that they can only be symmetric around the switching unit, making it difficult for example, to mix and match between chiral motifs that yield high β and $\Delta\beta$ values.[15]

Recently, we reported[16] on how the combination of bistable hydrazones[17] with a chiral isosorbide core results in a photoswitchable dopant that induces a cholesteric to smectic A transition in the LC host 5CB and enables the locking-in of different reflection wavelengths from the LC. Unfortunately, the β and $\Delta\beta$ values (57 and 22 μm^{-1}, respectively) of the dopant limited the system to only near-infrared light reflection, which while useful in certain applications, is constraining for others. On the other hand, when triptycene was recently used as the chiral motif in conjunction with the hydrazone photoswitch, higher β, and $\Delta\beta$ values were obtained, resulting in the reflection of visible color.[18] To better understand the factors that influence the β and $\Delta\beta$ values, we designed several iterations of the hydrazone-based isosorbide dopant, by varying the functionalization of the hydrazone rotor and/or stator phenyl groups (Schemes 1 and 2), the substitution of the isosorbide unit (2′ vs 5′ OH), and the number of chiral moieties. The goal of developing these dopants was to use structure−property analysis to tease out factors (e.g., nature of stereocenter, the effect of the number of chiral units, electronic effects, and so on) that govern their β and $\Delta\beta$ values. Here, we provide a detailed analysis using these new dopants and elaborate on the insights we learned, including new hypotheses, on how to design efficient switchable chiral LC dopants. We also show how once optimized these dopants can be used to control, and lock in for extended periods, the reflected color from LCs (from UV to the infrared region) as a function of either the photostationary state (PSS) or irradiation time at a particular wavelength.

RESULTS AND DISCUSSION

The photophysical data of compounds **1**−**16** are shown in Table S1 in the Supporting Information (see also Figures S65 and S129 for more details). In general, the switches with electron-donating and withdrawing groups result in the expected bathochromic and hypsochromic shifts, respectively. As previously shown,[17b] compounds bearing a *para*−NO_2 substitution at the stator phenyl group (e.g., **1**, **6**, and **7**) result in high PSSs and red-shifted absorption spectra. We attribute this outcome to a localized extended conjugation that yields a "quinoid" form involving the stator phenyl group and the hydrazone amine nitrogen. The thermal isomerization half-lives of the hydrazones were found to be between hundreds and thousands of years, and all the dopants show stability for many photoswitching cycles with minimal photodegradation (see Table S2).[17a]

The β values of the dopants in 5CB[19] at their 340 and 410 or 442 nm PSSs were measured using the Grandjean-Cano wedge method[20] and the results are summarized in Table 1.[21]

Scheme 1. Structures of Photochromic Dopants 1−7[a]

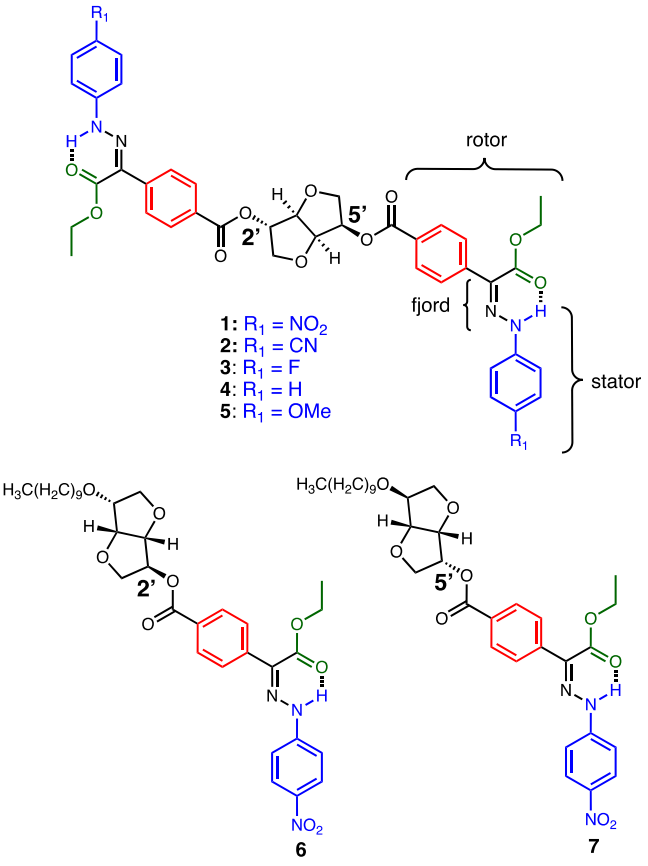

[a]Rotor and stator designations are arbitrary.

Scheme 2. Structures of Photochromic Dopants 8−16

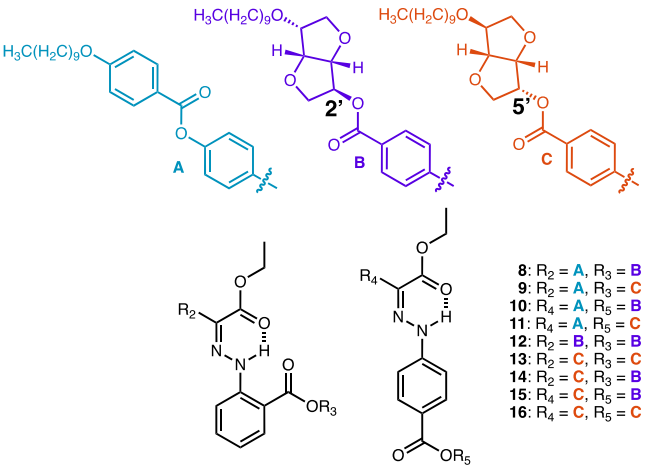

The β value of compounds **1**−**5**, which consist of two hydrazones connected to an isosorbide at the rotor phenyl portion, increases upon switching to the *E* form (in reality *EE* form but for the sake of clarity we will just use *E* and *Z* when appropriate), indicating that this isomer is interacting better with the chiral host. This observation is in line with other instances, where the *E* isomer resulted in better ordering in LC phases and polymeric systems.[16,22] Moreover, in all the dopants and no matter whether they are substituted with electron-donating or withdrawing groups, the *E* form has a higher β value, indicating that this phenomenon is not driven

https://doi.org/10.1021/jacs.4c07848
J. Am. Chem. Soc. 2024, 146, 24561−24569

Table 1. β Values (μm^{-1}) of Compounds 1−16 Recorded in Wedge Cells in 5CB at Room Temperature

dopant	β_Z	β_E	$\Delta\beta_{E\text{-}Z}$
1	<29[a]	94	+65
2	13	63	+50
3	61	106	+55
4	38	76	+38
5	17	73	+56
6	32	35	+3
7	13	32	+19
8	32	42	+10
9	47	40	−7
10	38	33	−5
11	54	54	+0
12	64	59	−5
13	76	82	+6
14	53	71	+18
15	37	69	+32
16	46	62	+16

[a]The β_Z value decreases to 29 μm^{-1} at PSS_{394} and below 10 μm^{-1} at PSS_{340}.

by electronic considerations. We speculate that the flexibility and rotational freedom of the *E* isomer, relative to the H-bonded, and hence, more rigid *Z* isomer, is responsible for this behavior (i.e., the *E* isomer can adopt a conformation that better interacts with the host LC). Importantly, this observation that flexibility in the fjord region (Scheme 1), and not rigidity, can result in better dopant-host interactions negates other empirical observations that show the opposite trend. This finding suggests that the generalization that rigidity results in large β values might not be universal.[23] It is worth noting that **3**, which has a *para*−F substituent, has the highest β value overall for both the *E* and *Z* isomers. It is known that fluorination of aromatic rings improves $\pi-\pi$ interactions,[24] and we speculate that this might be the reason for this observation (i.e., **3** interacts better with 5CB). Overall, the $\Delta\beta$ of **3** is comparable to the other derivatives because both the *E* and *Z* values increase in value relative to the others. In general, the β values of the *Z* isomers are comparably low indicating poorer interaction with the host LC. The exception is with unfunctionalized **4**, which has a relatively high β value in the *Z* form. This observation might indicate that the development of dipole moments through substitution in the other derivatives might contribute to the overall decrease in the β value. Finally, **1** has the largest $\Delta\beta$ in the series, and we attribute this result to a combination of two factors, flexibility and the above-mentioned "quinoid" resonance form. That is, being rigid and having a large dipole, which is what the "quinoid" form is, results in weak interactions with the host while in the *Z* form, whereas flexibility with a large dipole results in better interactions with the *E* isomer, resulting in the large $\Delta\beta$ value.

To better understand how the structural changes upon isomerization affect the β values, the *Z* and *E* isomers of compounds **1**−**5** were subjected to a gas-phase conformational analysis in which the lowest energy structure was then optimized by density functional theory (DFT) using the B3LYP[25] function with Grimme D3 dispersion correction[26] and the 6-31G** basis set.[27] Subsequent single-point calculations were performed using the 6-311G** basis set[28] using the Poisson−Boltzmann[29] continuum solvent model for

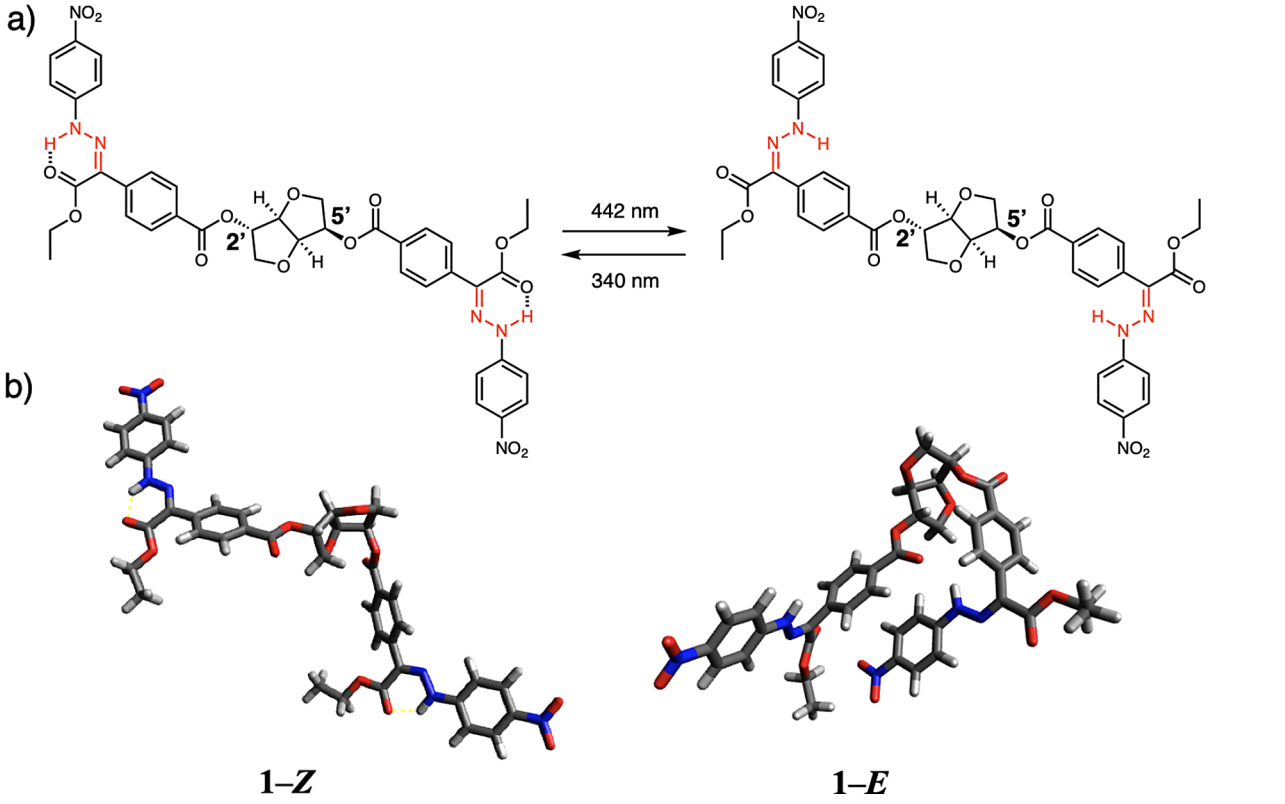

Figure 1. (a) Light-induced *Z*/*E* isomerization in **1**. The C═N−N−H bond is colored red to highlight the dihedral angle used in the analysis. (b) DFT (B3LYP/6-311G**)-calculated structures for **1**−*Z* and **1**−*E*.

https://doi.org/10.1021/jacs.4c07848
J. Am. Chem. Soc. 2024, 146, 24561−24569

dichloromethane (see the Supporting Information and Figures S155−S164).[30] A detailed analysis of the conformational and configurational space yielded minimum energy structures that shed light on the structural changes that result in large $\Delta\beta$ values. Compound **1**−***Z*** (Figure 1), which is used as a representative example of all other dopants, adopts a conformation in which the hydrazone switches are oriented away from each other in an *anti*-arrangement. Upon photoisomerization, the two hydrazone switches in **1**−***E*** are brought closer in proximity to each other in a *syn*-fashion. This change in conformation results in an increase in the β value and subsequently the $\Delta\beta$ value and suggests that the two hydrazone units in the *syn*-form are working together to facilitate better interactions with 5CB.

To get a better understanding of this observation, the β values of compounds **6** and **7**, which are model subunits of **1** were measured (Table 1). The comparison of these systems shows that there is a positive cooperative effect in the latter that is driving the β values higher in the *E* isomers, in accordance with the DFT calculation results. On the other hand, the hydrazones are acting independently in the *Z* isomer of **1** resulting in similar values to that of **7**. These trends seem to also capture what is happening in dopants **2**−**5**. Compounds **6** and **7** also show a trend that already became evident with dopants **1**−**5**; while long alkyl chains might help with solubility and dispersion interactions, they do not necessarily contribute to increasing the β values in these systems. This conclusion is contrary to the accepted empirical wisdom in the literature about the benefits of such alkyl chains.[31] Moreover, and when compared with the recently reported triptycene-based hydrazone dopants,[18] the effect seems to emerge not from the switch itself as it is the same in both dopant families, but from the chiral unit and most likely the shape it adopts (e.g., the triptycene most likely will not adopt the *anti*/*syn* conformation observed here). The substitution position of the isosorbide at the rotor portion of the hydrazone, whether at the 2′ or 5′ position (**6** or **7**, respectively), surprisingly also has a pronounced effect on the β value. The 2′ substitution results in a minimal change in the value upon $Z \rightarrow E$ photoisomerization, whereas the 5′ substitution results in an increase in the value. These results showcase that the nature of point chirality also plays a role in determining the β value.

Dopants **8**−**11** were designed to study the effect of *ortho*/*para* substitution of the stator phenyl group with the isosorbide unit at either the 2′ or 5′ positions (see Scheme 2). The comparison of these dopants shows that when at the *ortho* position the 2′ substitution gives smaller β values for the *Z* isomer and similar values for the *E* isomer when compared to the 5′ substitution. On the other hand, when at the *para* position, the *E* and *Z* isomers interact better with the LC host when in a 5′ substitution vs 2′ substitution pattern, and hence, have larger β values. Interestingly, compound **11** shows a minimal $\Delta\beta$ for both isomers. Based on this analysis and compared with dopants **8** and **10**, the low β value for the *Z* isomer in **7** seems to originate from the 5′ isosorbide substitution being at the rotor phenyl group rather than solely the 5′ substitution of isosorbide.

Dopants **12** and **13** comprise a hydrazone connected at the rotor and stator (*ortho*) with two isosorbide units substituted at the 2′ or 5′ positions, respectively. When comparing the β value of **12** with that of **8** it is evident that each isosorbide is acting separately and resulting in a straightforward additive effect, i.e., the value of **12** that has two isosorbides is double that of **8** which has one such unit. Comparing **13** and **9** shows a couple of interesting phenomena. First, there is a positive cooperativity effect, as the β values of the double isosorbide system are more than double that of the single isosorbide dopant affords. Second, having the stator functionalized with the isosorbide unit substituted at the 5′ position drastically increases the β value of the *Z* isomer, as can also be observed when comparing **8** with **9** and **10** with **11**. To take advantage of these insights (Scheme 3) we designed dopant **14** in which

Scheme 3. Visual Representation of the Structural Changes that Lead to Large $\Delta\beta$ Values

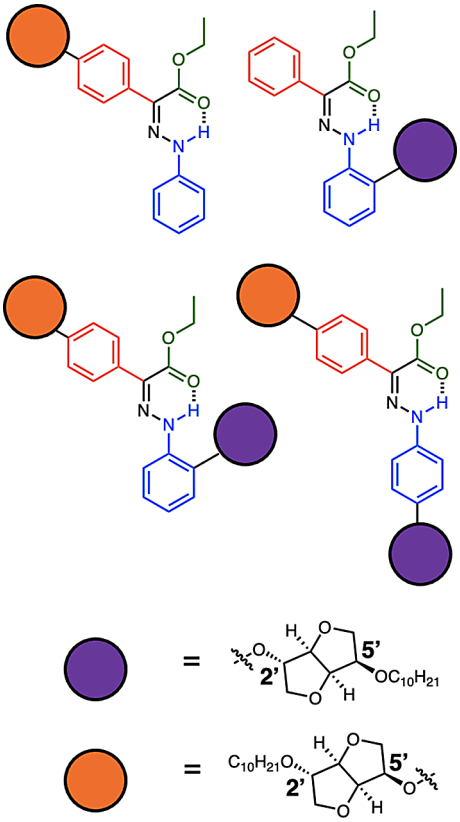

the isosorbide is attached to the rotor at the 5′ position, while the stator is attached at the 2′ position. The substitution pattern indeed resulted in the largest $\Delta\beta$ value in the *ortho*-substituted series. Interestingly, the β value of the *E* isomer is an average of what is observed in **12** and **13**, giving further evidence of an additive effect. The *Z* isomer result on the other hand indicates that there is negative cooperativity, as the value is lower in **14** than in **12** and **13**. Lower β values for the *Z* isomer of **8** were also observed in comparison to **9** indicating that the decrease in interaction in **14** originates from the 2′ isosorbide substitution at the stator phenyl. Next, we studied the effect of having the isosorbide at the *para* position of the stator phenyl group using dopants **15** and **16**. In general, these dopants show larger $\Delta\beta$ values in comparison with those of the *ortho*-substituted systems **12**−**14**. The comparison between **15** and **16**, which vary only in the isosorbide substitution position (2′ vs 5′ at the stator phenyl group while the rotor is the same), shows that the large $\Delta\beta$ value stems from the *Z* isomer which has lower β values. This result means that the *Z* isomer in **12**−**14** interacts better when the isosorbide is at the *ortho* position. Finally, a comparison of **13** and **16** (5′ substitution at

https://doi.org/10.1021/jacs.4c07848
J. Am. Chem. Soc. 2024, 146, 24561−24569

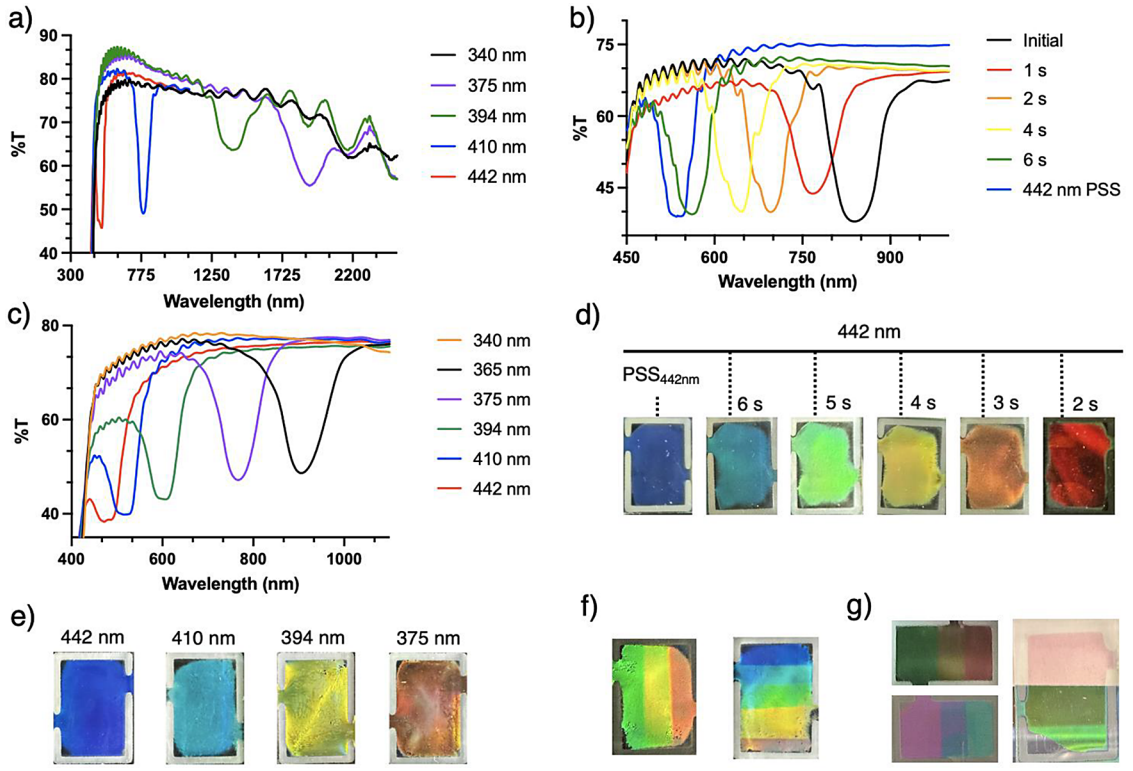

Figure 2. Transmittance spectra and micrograph images of reflective films of hydrazone dopants in LC host 5CB. (a) Reflectance modulation using **1** (3.5 mol % doping in 5CB) as a function of 340, 375, 394, 410, and 442 nm light irradiation; (b) reflectance modulation using **1** (3.0 mol % doping in 5CB) as a function of 442 nm light irradiation time and finally the PSS; (c) reflectance modulation using **3** (2.8 mol % doping in 5CB) as a function of 340, 365, 375, 394, 410, and 442 nm light irradiation; (d) micrograph images of reflective films using **1** (3.5 mol % doping in 5CB) as a function of 442 light irradiation time to reach PSS_{442}; (e) micrograph images of reflective films using **3** (2.8 mol % doping in 5CB) as a function of the wavelength dependent PSS; (f) micrograph images of masked reflective films showing how different colors can be locked-in for multiple days, in the same film, as a function of irradiation time (on the left) using **1** (3.5 mol % doping in 5CB) or PSS (on the right) using **3** (2.8 mol % doping in 5CB); and (g) micrograph images of masked reflective films using **8** (7.5 mol % doping in 5CB) against a black or white background.

the rotor and the *ortho* or *para* positions of the stator phenyl) shows that both the *Z* and *E* isomers are interacting less efficiently in the *para* derivative. The β values for the *Z* and *E* isomers of **13** are 76 and 82 μm^{-1}, whereas for **16**, the β values are 46 and 62 μm^{-1}. Dopant **16** shows much weaker LC host interactions for the *Z* isomer when compared to the *E* isomer resulting in a much larger $\Delta\beta$, whereas **13** shows similar interactions with the LC host for both isomers.

The DFT calculated structures of the *Z* and *E* isomers for **8**−**16** unfortunately did not show large conformational differences that can explain these observed trends (see Figures S165 and S182 for more details). These calculations still gave us an insight into a structural factor that controls the $\Delta\beta$ value, the hydrazone CNNH dihedral angle. We discovered that when this angle increases upon photoisomerization, then the $\Delta\beta$ value increases as well and vice versa (Table S3).[32] For example, in **12**, the dihedral angle decreases from 5.24° to 3.98° upon isomerization which results in a $\Delta\beta$ value of −5 μm^{-1}, whereas in **14** the dihedral angle increases from 3.57° to 4.72° resulting in a $\Delta\beta$ value of +18 μm^{-1}. This finding, which can be used to accurately predict the trend in 12 out of the 14 dopants that were calculated, indicates that this portion of the hydrazone core is involved in facilitating the interaction with the host 5CB.

We next took advantage of the bistability of the hydrazone, and relatively large β and $\Delta\beta$ values of the dopants to kinetically trap the self-assembled cholesteric phase, and hence, reflected wavelength/color in 5CB films (Table 1). Dopant **1**, which exhibits the largest $\Delta\beta$ upon photoisomerization, showed a phenomenal change in reflected light wavelength upon photoswitching, ranging from 450 to >1930 nm (Figure 2a). Surprisingly, the 10% difference (Figure S67) in the *E*:*Z* isomer ratio when going from PSS_{442} to PSS_{410} resulted in a 58% decrease in the β value (Figure S130) and a 350 nm bathochromic shift in the transmittance spectrum. This phenomenon allowed us to control the reflectance wavelength from the visible, which was not possible with our previously reported hydrazone/isosorbide dopant, to the NIR range. Such a large change from a small variation in PSS though is not adequate for accurate control over the reflected colors. Hence, to enhance control accuracy, we decided to lock in the reflected colors as a function of irradiation time at a particular wavelength. We chose 442 nm for this demonstration (Figure 2b) and showed that this approach yields better control over the reflected colors (Figure 2d). Switching the dopant with 394 nm light surprisingly shifts the reflectance to 1500 nm, while 375 nm pushes it further to 1930 nm. Shorter irradiation wavelengths shift the reflectance further into the NIR > 2000 nm. Unfortunately, we could not measure these, because of the limitation of our spectrophotometer. We speculate that the push−pull nature of **1** and the large dipole moment it results in is responsible for its ability to attenuate the reflection wavelength to such an extent.

Reflected light could not be generated from dopant **2** in planar cells as it exhibited parallel alignment issues, presumably from anchoring effects. Dopant **3** on the other hand resulted in

https://doi.org/10.1021/jacs.4c07848
J. Am. Chem. Soc. 2024, 146, 24561−24569

wavelength reflectance ranging from 450 to 930 nm (Figure 2c), which we used to reversibly lock in various reflected colors (Figure 2e) including the primary ones (red, green, and blue when relying on irradiation time (Figure 2d)). We also used simple masks to show how different color reflections can be programmed on the same LC film (Figure 2f). Similar results were obtained for dopant **8** (Figure 2g). The data for the rest of the dopants are summarized in Table 2.

Table 2. Reflectance Wavelength Range Recorded for Hydrazone Dopants in 5CB

dopant	reflectance wavelength range (nm)
1	450−1930
2[a]	700−800
3	450−930
4	675−1075
5	800−1050
8	540−730
10	775−950
16	710−1075

[a]Reflectance of Compound **2** was measured in a homeotropic E47 cell.[33]

CONCLUSIONS

In conclusion, 16 new hydrazone dopants containing isosorbide moieties were synthesized and analyzed to better understand how the structure of the dopant affects its β and $\Delta\beta$ values. The new dopants were also used in modulating and locking in different visible colors from LC films as a function of irradiation time or wavelength-dependent PSS. The majority of the newly developed hydrazone dopants show a larger β value in the *E* form rather than the *Z* one, which is the trend observed in previously studied LC hydrazone dopants containing isosorbide[16] and triptycene[18] moieties. We show here that this phenomenon, which goes against accepted rules of thumb related to dopant rigidity, has to do with the CNNH dihedral angle. Dopant **1**, which also does not abide by the usual rule of thumb requiring alkoxy chains for optimizing properties, results in phenomenal control (>1500 nm covering the visible to NIR region) over the reflectance wavelength. Finally, it is worth emphasizing that the straightforward synthesis of these switches allows access to nonsymmetric dopants with enhanced qualities through the mixing and matching of different structural properties (e.g., which substitution pattern yields larger β and $\Delta\beta$ values), which is not trivial using other photoswitchable dopants.[14]

Based on the structure−property analysis (Scheme 3) the following rules of thumb can be used when designing future hydrazone-containing isosorbide-based chiral dopants: (1) alkoxy chains are not necessary for increasing the solubility of the dopant and its interactions with the host LC, i.e., increasing β values; (2) dopants with only rotor connectivity to the isosorbide unit result in larger $\Delta\beta$ values when 5′ substituted and smaller $\Delta\beta$ values when 2′ substituted; (3) substituting the stator (*ortho* or *para*) with isosorbide at the 2′ position results in larger $\Delta\beta$ values than at the 5′ one; (4) upon functionalization of the chiral moiety, the substitution position should be chosen to maximize the change in the CNNH dihedral angle upon isomerization, which will result in higher β values; (5) unsymmetric substitution (5′,2′) of flanking isosorbides (switch in the middle) leads to larger $\Delta\beta$ values than when substitutions are at the same position (5′,5′ and 2′,2′). (6) Although increasing the number of chiral units does appear to have an additive effect on the β value, this does not translate into a large $\Delta\beta$ value. Instead, dopants should be designed such that one central chiral moiety is attached to the rotor part of two hydrazones to maximize the interactions with the LC and obtain large $\Delta\beta$ values. These qualitative insights will help us and others in designing better dopants that can be used in controlling and modulating the β and $\Delta\beta$ values of chiral dopants so they can be applied in the design of new LC-based adaptive soft materials.[34]

ASSOCIATED CONTENT

Supporting Information

The Supporting Information is available free of charge at https://pubs.acs.org/doi/10.1021/jacs.4c07848.

General methods, experimental procedures, NMR spectra of key compounds, photoisomerization studies, kinetic studies, details about doping experiments, and DFT calculations (PDF)

AUTHOR INFORMATION

Corresponding Author

Ivan Aprahamian − *Department of Chemistry, Dartmouth College, Hanover, New Hampshire 03755, United States;* orcid.org/0000-0003-2399-8208; Email: ivan.aprahamian@dartmouth.edu

Authors

Brandon Balamut − *Department of Chemistry, Dartmouth College, Hanover, New Hampshire 03755, United States*

Russell P. Hughes − *Department of Chemistry, Dartmouth College, Hanover, New Hampshire 03755, United States*

Complete contact information is available at: https://pubs.acs.org/10.1021/jacs.4c07848

Notes

The authors declare no competing financial interest.

ACKNOWLEDGMENTS

This work was supported by the NSF program (DMR-2104464). RPH thanks Dartmouth College Research Computing for assistance with software acquisition.

REFERENCES

(1) (a) Ichimura, K. Photoalignment of Liquid-Crystal Systems. *Chem. Rev.* **2000**, *100*, 1847−1874. (b) Wang, Y.; Li, Q. Light-Driven Chiral Molecular Switches or Motors in Liquid Crystals. *Adv. Mater.* **2012**, *24*, 1926−1945. (c) Wang, D.; Park, S.-Y.; Kang, I.-K. Liquid Crystals: Emerging Materials for Use in Real-Time Detection Applications. *J. Mater. Chem. C* **2015**, *3*, 9038−9047. (d) Oladepo, S. A. Development and Application of Liquid Crystals as Stimuli-Responsive Sensors. *Molecules* **2022**, *27*, 1453. (e) Braganza, C.; Echeverri, M. Bistable Cholesteric Liquid Crystal Displays − Review and Writing Tablets. In *E-Paper Displays*; Yang, B., Ed.; Wiley, 2022; pp 99−129.

(2) (a) Demus, D. Chemical Structure and Mesogenic Properties. *In Handbook of Liquid Crystals Set*; Demus, D.; Goodby, J.; Gray, G. W.; Spiess, H.-W.; Vill, V., Eds.; Wiley-VCH Verlag GmbH: Weinheim, Germany, 1998; pp 133−187. (b) Kinoshita, S.; Yoshioka, S. Structural Colors in Nature: The Role of Regularity and Irregularity in the Structure. *ChemPhysChem* **2005**, *6*, 1442−1459. (c) de Gennes, P.-G.; Prost, J. *The Physics of Liquid Crystals*, 2nd ed., repr.; International Series of Monographs on Physics; Clarendon Press:

Oxford, 2013; pp 3−18. (d) Geelhaar, T.; Griesar, K.; Reckmann, B. 125 Years of Liquid Crystals-A Scientific Revolution in the Home. *Angew. Chem., Int. Ed.* **2013**, *52*, 8798−8809. (e) Bisoyi, H. K.; Li, Q. Liquid Crystals: Versatile Self-Organized Smart Soft Materials. *Chem. Rev.* **2022**, *122*, 4887−4926. (f) *Molecular Photoswitches: Chemistry, Properties, and Applications*; Pianowski, Z. L., Ed.; Wiley-VCH: Weinheim, 2022; pp 214−243.

(3) (a) Li, Q.; Li, Y.; Ma, J.; Yang, D.-K.; White, T. J.; Bunning, T. J. Directing Dynamic Control of Red, Green, and Blue Reflection Enabled by a Light-Driven Self-Organized Helical Superstructure. *Adv. Mater.* **2011**, *23*, 5069−5073. (b) Kim, Y.; Tamaoki, N. A Photoresponsive Planar Chiral Azobenzene Dopant with High Helical Twisting Power. *J. Mater. Chem. C* **2014**, *2*, 9258−9264. (c) Wang, Y.; Zheng, Z.; Bisoyi, H. K.; Gutierrez-Cuevas, K. G.; Wang, L.; Zola, R. S.; Li, Q. Thermally Reversible Full Color Selective Reflection in a Self-Organized Helical Superstructure Enabled by a Bent-Core Oligomesogen Exhibiting a Twist-Bend Nematic Phase. *Mater. Horiz.* **2016**, *3*, 442−446. (d) Wang, H.; Bisoyi, H. K.; Wang, L.; Urbas, A. M.; Bunning, T. J.; Li, Q. Photochemically and Thermally Driven Full-Color Reflection in a Self-Organized Helical Superstructure Enabled by a Halogen-Bonded Chiral Molecular Switch. *Angew. Chem., Int. Ed.* **2018**, *57*, 1627−1631. (e) Qin, L.; Gu, W.; Wei, J.; Yu, Y. Piecewise Phototuning of Self-Organized Helical Superstructures. *Adv. Mater.* **2018**, *30*, 1704941. (f) Hou, J.; Long, G.; Zhao, W.; Zhou, G.; Liu, D.; Broer, D. J.; Feringa, B. L.; Chen, J. Phototriggered Complex Motion by Programmable Construction of Light-Driven Molecular Motors in Liquid Crystal Networks. *J. Am. Chem. Soc.* **2022**, *144*, 6851−6860. (g) Hou, J.; Toyoda, R.; Meskers, S. C. J.; Feringa, B. L. Programming and Dynamic Control of the Circular Polarization of Luminescence from an Achiral Fluorescent Dye in a Liquid Crystal Host by Molecular Motors. *Angew. Chem. Int. Ed* **2022**, *61*, No. e202206310.

(4) (a) Popov, P.; Mann, E. K.; Jákli, A. Thermotropic Liquid Crystal Films for Biosensors and Beyond. *J. Mater. Chem. B* **2017**, *5*, 5061−5078. (b) Oh, S.-W.; Kim, S.-H.; Yoon, T.-H. Thermal Control of Transmission Property by Phase Transition in Cholesteric Liquid Crystals. *J. Mater. Chem. C* **2018**, *6*, 6520−6525. (c) Oswald, P.; Dequidt, A.; Poy, G. Lehmann Effect in Nematic and Cholesteric Liquid Crystals: A Review. *Liquid Crystals Reviews* **2019**, *7*, 142−166. (d) Zhang, W.; Froyen, A. A. F.; Schenning, A. P. H. J.; Zhou, G.; Debije, M. G.; De Haan, L. T. Temperature-Responsive Photonic Devices Based on Cholesteric Liquid Crystals. *Adv. Photo Res.* **2021**, *2*, 2100016. (e) Labeeb, A. M.; Ward, Y. A.; Fikry, M. Thermal Control of Tunable Photonic Optical Bandgaps in Different Cholesteric Liquid Crystals Mixtures. *J. Mol. Liq.* **2021**, *340*, No. 117179.

(5) (a) Aprahamian, I.; Yasuda, T.; Ikeda, T.; Saha, S.; Dichtel, W. R.; Isoda, K.; Kato, T.; Stoddart, J. F. A Liquid-Crystalline Bistable [2]Rotaxane. *Angew. Chem., Int. Ed.* **2007**, *46*, 4675−4679. (b) Tan, B.-H.; Yoshio, M.; Kato, T. Induction of Columnar and Smectic Phases for Spiropyran Derivatives: Effects of Acidichromism and Photochromism. *Chemistry - An Asian Journal* **2008**, *3*, 534−541. (c) Yasuda, T.; Tanabe, K.; Tsuji, T.; Coti, K. K.; Aprahamian, I.; Stoddart, J. F.; Kato, T. A Redox-Switchable [2]Rotaxane in a Liquid-Crystalline State. *Chem. Commun.* **2010**, *46*, 1224. (d) Sakuda, J.; Yasuda, T.; Kato, T. Liquid-Crystalline Catenanes and Rotaxanes. *Isr. J. Chem.* **2012**, *52*, 854−862. (e) Su, X.; Voskian, S.; Hughes, R. P.; Aprahamian, I. Manipulating Liquid-Crystal Properties Using a pH Activated Hydrazone Switch. *Angew. Chem., Int. Ed.* **2013**, *52*, 10734−10739. (f) Katsonis, N.; Lancia, F.; Leigh, D. A.; Pirvu, L.; Ryabchun, A.; Schaufelberger, F. Knotting a Molecular Strand Can Invert Macroscopic Effects of Chirality. *Nat. Chem.* **2020**, *12*, 939−944.

(6) (a) Tondiglia, V. P.; Rumi, M.; Idehenre, I. U.; Lee, K. M.; Binzer, J. F.; Banerjee, P. P.; Evans, D. R.; McConney, M. E.; Bunning, T. J.; White, T. J. Electrical Control of Unpolarized Reflectivity in Polymer-Stabilized Cholesteric Liquid Crystals at Oblique Incidence. *Adv. Opt. Mater.* **2018**, *6*, 1800957. (b) Krakhalev, M. N.; Prishchepa, O. O.; Sutormin, V. S.; Bikbaev, R. G.; Timofeev, I. V.; Zyryanov, V. Ya. Electrically Induced Transformations of Defects in Cholesteric Layer with Tangential-Conical Boundary Conditions. *Sci. Rep* **2020**, *10*, 4907. (c) Prishchepa, O.; Krakhalev, M.; Rudyak, V.; Sutormin, V.; Zyryanov, V. Electrically Turning Periodic Structures in Cholesteric Layer with Conical−Planar Boundary Conditions. *Sci. Rep* **2021**, *11*, 8409. (d) Gu, C.; Jia, A.-B.; Zhang, Y.-M.; Zhang, S. X.-A. Emerging Electrochromic Materials and Devices for Future Displays. *Chem. Rev.* **2022**, *122*, 14679−14721. (e) Li, Z.; Lan, R.; Bao, J.; Hu, W.; Wang, M.; Zhang, L.; Yang, H. Tunable Circularly Polarized Luminescence with a High Dissymmetry Factor Emitted from Luminogen-Bonded and Electrically Controlled Polymer-Stabilized Cholesteric Liquid Crystals. *ACS Appl. Mater. Interfaces* **2022**, *14*, 8490−8498. (f) Lee, K. M.; Marsh, Z. M.; Crenshaw, E. P.; Tohgha, U. N.; Ambulo, C. P.; Wolf, S. M.; Carothers, K. J.; Limburg, H. N.; McConney, M. E.; Godman, N. P. Recent Advances in Electro-Optic Response of Polymer-Stabilized Cholesteric Liquid Crystals. *Materials* **2023**, *16*, 2248.

(7) (a) White, T. J.; McConney, M. E.; Bunning, T. J. Dynamic Color in Stimuli-Responsive Cholesteric Liquid Crystals. *J. Mater. Chem.* **2010**, *20*, 9832−9847. (b) Bisoyi, H. K.; Li, Q. Light-Driven Liquid Crystalline Materials: From Photo-Induced Phase Transitions and Property Modulations to Applications. *Chem. Rev.* **2016**, *116*, 15089−15166. (c) Wang, L.; Li, Q. Photochromism into Nanosystems: Towards Lighting up the Future Nanoworld. *Chem. Soc. Rev.* **2018**, *47*, 1044−1097. (d) Kim, Y.; Tamaoki, N. Photoresponsive Chiral Dopants: Light-Driven Helicity Manipulation in Cholesteric Liquid Crystals for Optical and Mechanical Functions. *ChemPhotoChem.* **2019**, *3*, 284−303. (e) Lan, R.; Bao, J.; Li, Z.; Wang, Z.; Song, C.; Shen, C.; Huang, R.; Sun, J.; Wang, Q.; Zhang, L.; Yang, H. Orthogonally Integrating Programmable Structural Color and Photo-Rewritable Fluorescence in Hydrazone Photoswitch-bonded Cholesteric Liquid Crystalline Network. *Angew. Chem., Int. Ed.* **2022**, *61*, No. e202213915.

(8) (a) Bobrovsky, A.; Ryabchun, A.; Cigl, M.; Hamplová, V.; Kašpar, M.; Hampl, F.; Shibaev, V. New Azobenzene-Based Chiral-Photochromic Substances with Thermally Stable Z-Isomers and Their Use for the Induction of a Cholesteric Mesophase with a Phototunable Helix Pitch. *J. Mater. Chem. C* **2014**, *2*, 8622−8629. (b) Wang, L.; Chen, D.; Gutierrez-Cuevas, K. G.; Krishna Bisoyi, H.; Fan, J.; Zola, R. S.; Li, G.; Urbas, A. M.; Bunning, T. J.; Weitz, D. A.; Li, Q. Optically Reconfigurable Chiral Microspheres of Self-Organized Helical Superstructures with Handedness Inversion. *Mater. Horiz.* **2017**, *4*, 1190−1195. (c) Huang, H.; Orlova, T.; Matt, B.; Katsonis, N. Long-Lived Supramolecular Helices Promoted by Fluorinated Photoswitches. *Macromol. Rapid Commun.* **2018**, *39*, No. 1700387. (d) Kim, Y.; Mafy, N. N.; Maisonneuve, S.; Lin, C.; Tamaoki, N.; Xie, J. Glycomacrocycle-Based Azobenzene Derivatives as Chiral Dopants for Photoresponsive Cholesteric Liquid Crystals. *ACS Appl. Mater. Interfaces* **2020**, *12*, 52146−52155. (e) Wang, Q.; Chen, H.; Xing, H.; Deng, Y.; Luo, Z.-W.; Xie, H.-L. Long Rod-Like Liquid Crystal Containing Azobenzene and the Applications in Phase-Transition Regulation and Orientation of Nematic Liquid Crystal. *Crystals* **2021**, *11*, 418.

(9) (a) Li, Y.; Wang, M.; Urbas, A.; Li, Q. A Photoswitchable and Thermally Stable Axially Chiral Dithienylperfluorocyclopentene Dopant with High Helical Twisting Power. *J. Mater. Chem. C* **2013**, *1*, 3917−3923. (b) Li, Y.; Wang, M.; Wang, H.; Urbas, A.; Li, Q. Rationally Designed Axially Chiral Diarylethene Switches with High Helical Twisting Power. *Chem.—Eur. J.* **2014**, *20*, 16286−16292. (c) Irie, M.; Fukaminato, T.; Matsuda, K.; Kobatake, S. Photochromism of Diarylethene Molecules and Crystals: Memories, Switches, and Actuators. *Chem. Rev.* **2014**, *114*, 12174−12277. (d) Bisoyi, H. K.; Li, Q. Light-Directed Dynamic Chirality Inversion in Functional Self-Organized Helical Superstructures. *Angew. Chem., Int. Ed.* **2016**, *55*, 2994−3010. (e) Zheng, Z.; Li, Y.; Bisoyi, H. K.; Wang, L.; Bunning, T. J.; Li, Q. Three-Dimensional Control of the Helical Axis of a Chiral Nematic Liquid Crystal by Light. *Nature* **2016**, *531*, 352−356. (f) Zheng, Z.; Hu, H.; Zhang, Z.; Liu, B.; Li, M.; Qu, D.-H.; Tian, H.; Zhu, W.-H.; Feringa, B. L. Digital Photo-

https://doi.org/10.1021/jacs.4c07848
J. Am. Chem. Soc. 2024, 146, 24561−24569

programming of Liquid-Crystal Superstructures Featuring Intrinsic Chiral Photoswitches. *Nat. Photonics* **2022**, *16*, 226−234.
(10) Herder, M.; Schmidt, B. M.; Grubert, L.; Pätzel, M.; Schwarz, J.; Hecht, S. Improving the Fatigue Resistance of Diarylethene Switches. *J. Am. Chem. Soc.* **2015**, *137*, 2738−2747.
(11) (a) Li, J.; Bisoyi, H. K.; Tian, J.; Guo, J.; Li, Q. Optically Rewritable Transparent Liquid Crystal Displays Enabled by Light-Driven Chiral Fluorescent Molecular Switches. *Adv. Mater.* **2019**, *31*, No. 1807751. (b) He, Y.; Zhang, S.; Bisoyi, H. K.; Qiao, J.; Chen, H.; Gao, J.; Guo, J.; Li, Q. Irradiation-Wavelength Directing Circularly Polarized Luminescence in Self-Organized Helical Superstructures Enabled by Hydrogen-Bonded Chiral Fluorescent Molecular Switches. *Angew. Chem. Int. Ed* **2021**, *60*, 27158−27163. (c) Kang, W.; Tang, Y.; Meng, X.; Lin, S.; Zhang, X.; Guo, J.; Li, Q. A Photo- and Thermo-Driven Azoarene-Based Circularly Polarized Luminescence Molecular Switch in a Liquid Crystal Host. *Angew. Chem. Int. Ed* **2023**, *62*, No. e202311486. (d) Liu, J.; Song, Z.; Sun, L.; Li, B.; Lu, Y.; Li, Q. Circularly Polarized Luminescence in Chiral Orientationally Ordered Soft Matter Systems. *Responsive Materials* **2023**, *1*, No. e20230005. (e) Wang, H.; Tang, Y.; Krishna Bisoyi, H.; Li, Q. Reversible Handedness Inversion and Circularly Polarized Light Reflection Tuning in Self-Organized Helical Superstructures Using Visible-Light-Driven Macrocyclic Chiral Switches. *Angew. Chem. Int. Ed* **2023**, *62*, No. e202216600.
(12) Ma, L.; Hu, W.; Zheng, Z.; Wu, S.; Chen, P.; Li, Q.; Lu, Y. Light-Activated Liquid Crystalline Hierarchical Architecture Toward Photonics. *Adv. Opt. Mater.* **2019**, *7*, No. 1900393.
(13) Goh, M.; Akagi, K. Powerful Helicity Inducers: Axially Chiral Binaphthyl Derivatives. *Liq. Cryst.* **2008**, *35*, 953−965.
(14) (a) Hayasaka, H.; Miyashita, T.; Nakayama, M.; Kuwada, K.; Akagi, K. Dynamic Photoswitching of Helical Inversion in Liquid Crystals Containing Photoresponsive Axially Chiral Dopants. *J. Am. Chem. Soc.* **2012**, *134*, 3758−3765. (b) Li, Y.; Xue, C.; Wang, M.; Urbas, A.; Li, Q. Photodynamic Chiral Molecular Switches with Thermal Stability: From Reflection Wavelength Tuning to Handedness Inversion of Self-Organized Helical Superstructures. *Angew. Chem., Int. Ed.* **2013**, *52*, 13703−13707. (c) Wang, L.; Dong, H.; Li, Y.; Liu, R.; Wang, Y.-F.; Bisoyi, H. K.; Sun, L.-D.; Yan, C.-H.; Li, Q. Luminescence-Driven Reversible Handedness Inversion of Self-Organized Helical Superstructures Enabled by a Novel Near-Infrared Light Nanotransducer. *Adv. Mater.* **2015**, *27*, 2065−2069.
(15) (a) Hou, J.; Mondal, A.; Long, G.; Haan, L.; Zhao, W.; Zhou, G.; Liu, D.; Broer, D. J.; Chen, J.; Feringa, B. L. Photo-responsive Helical Motion by Light-Driven Molecular Motors in a Liquid-Crystal Network. *Angew. Chem., Int. Ed.* **2021**, *60*, 8251−8257. (b) Ishihara, S.; Uto, S. Symmetry and Liquid Crystals. *Symmetry* **2023**, *15*, 691.
(16) Moran, M. J.; Magrini, M.; Walba, D. M.; Aprahamian, I. Driving a Liquid Crystal Phase Transition Using a Photochromic Hydrazone. *J. Am. Chem. Soc.* **2018**, *140*, 13623−13627.
(17) (a) Qian, H.; Pramanik, S.; Aprahamian, I. Photochromic Hydrazone Switches with Extremely Long Thermal Half-Lives. *J. Am. Chem. Soc.* **2017**, *139*, 9140−9143. (b) Shao, B.; Qian, H.; Li, Q.; Aprahamian, I. Structure Property Analysis of the Solution and Solid-State Properties of Bistable Photochromic Hydrazones. *J. Am. Chem. Soc.* **2019**, *141*, 8364−8371. (c) Shao, B.; Aprahamian, I. Hydrazones as New Molecular Tools. *Chem.* **2020**, *6*, 2162−2173. (d) Qiu, Q.; Yang, S.; Gerkman, M. A.; Fu, H.; Aprahamian, I.; Han, G. G. D. Photon Energy Storage in Strained Cyclic Hydrazones: Emerging Molecular Solar Thermal Energy Storage Compounds. *J. Am. Chem. Soc.* **2022**, *144*, 12627−12631. (e) Thaggard, G. C.; Leith, G. A.; Sosnin, D.; Martin, C. R.; Park, K. C.; McBride, M. K.; Lim, J.; Yarbrough, B. J.; Maldeni Kankanamalage, B. K. P.; Wilson, G. R.; Hill, A. R.; Smith, M. D.; Garashchuk, S.; Greytak, A. B.; Aprahamian, I.; Shustova, N. B. Confinement-Driven Photophysics in Hydrazone-Based Hierarchical Materials. *Angew. Chem. Int. Ed* **2023**, *62*, No. e202211776.
(18) Bala, I.; Plank, J. T.; Balamut, B.; Henry, D.; Lippert, A. R.; Aprahamian, I. Multistage and Multicolor Liquid Crystal Reflections using a Chiral Triptycene Photoswitchable Dopant. Accepted in principle by *Nature Chem.* 2024. Original version uploaded to ChemRxiv DOI: 10.26434/chemrxiv-2024-rcvcc.
(19) We screened a number of host LCs including E7 and found that 5CB, which is widely used in such studies, gives the best results.
(20) Tang, T.-T.; Wu, H.-Y.; Lin, C.-J.; Pan, R.-P. A Simple Method of Determining the Pitch of a Chiral Nematic Liquid Crystal. *Mol. Cryst. Liq. Cryst.* **2007**, *478*, 143−150.
(21) The concentration (n) of the dopant is chosen such that it induces a similar helical pitch (p) of the LC phase as the wavelength of light (λ) we wish to reflect based on the relation: $\lambda = np$.
(22) Yang, S.; Harris, J. D.; Lambai, A.; Jeliazkov, L. L.; Mohanty, G.; Zeng, H.; Priimagi, A.; Aprahamian, I. Multistage Reversible T_g Photomodulation and Hardening of Hydrazone-Containing Polymers. *J. Am. Chem. Soc.* **2021**, *143*, 16348−16353.
(23) (a) Neal, M. P.; Solymosi, M.; Wilson, M. R.; Earl, D. J. Helical Twisting Power and Scaled Chiral Indices. *J. Chem. Phys.* **2003**, *119*, 3567−3573. (b) Wang, X.; He, J.; Wei, Q.; Zhang, Y.; Li, Y.; Zhang, Z.; Zhao, W.; Zhou, G. Influence of Molecular Weight on Helical Twisting Power of Oligomer Chiral Dopants. *J. Mol. Liq.* **2021**, *339*, No. 116816. (c) Hussain, S.; Zourob, M. Solid-State Cholesteric Liquid Crystals as an Emerging Platform for the Development of Optical Photonic Sensors. *Small* **2023**, *20*, No. 2304590.
(24) (a) Reichenbächer, K.; Süss, H. I.; Hulliger, J. Fluorine in Crystal Engineering—"the Little Atom That Could. *Chem. Soc. Rev.* **2005**, *34*, 22−30. (b) Babudri, F.; Farinola, G. M.; Naso, F.; Ragni, R. Fluorinated Organic Materials for Electronic and Optoelectronic Applications: The Role of the Fluorine Atom. *Chem. Commun.* **2007**, *10*, 1003−1022.
(25) (a) Andersson, M. P.; Uvdal, P. New scale factors for harmonic vibrational frequencies using the B3LYP density functional method with the triple-zeta basis set 6-311+G(d,p). *J. Phys. Chem. A* **2005**, *109*, 2937−2941. (b) Stephens, P. J.; Devlin, F. J.; Chabalowski, C. F.; Frisch, M. J. Ab Initio Calculation of Vibrational Absorption and Circular Dichroism Spectra Using Density Functional Force Fields. *J. Phys. Chem.* **1994**, *98*, 11623−11627. (c) Becke, A. D. A new mixing of Hartree-Fock and local-density-functional theories. *J. Chem. Phys.* **1993**, *98*, 1372−1377. (d) Becke, A. D. Density-functional thermochemistry. III. The role of exact exchange. *J. Chem. Phys.* **1993**, *98*, 5648−5652. (e) Lee, C.; Yang, W.; Parr, R. G. Development of the Colle-Salvetti correlation-energy formula into a functional of the electron density. *Phys. Rev. B* **1988**, *37*, 785−789.
(26) (a) Goerigk, L.; Grimme, S. A thorough benchmark of density functional methods for general main group thermochemistry, kinetics, and noncovalent interactions. *Phys. Chem. Chem. Phys.* **2011**, *13*, 6670−6688. (b) Grimme, S.; Antony, J.; Ehrlich, S.; Krieg, H. A consistent and accurate ab initio parametrization of density functional dispersion correction (DFT-D) for the 94 elements H-Pu. *J. Chem. Phys.* **2010**, *132*, No. 154104.
(27) (a) Francl, M. M.; Pietro, W. J.; Hehre, W. J.; Binkley, J. S.; Gordon, M. S.; DeFrees, D. J.; Pople, J. A. Self-consistent molecular orbital methods. XXIII. A polarization-type basis set for second-row elements. *J. Chem. Phys.* **1982**, *77*, 3654−3665. (b) Binkley, J. S.; Pople, J. A. Self-consistent molecular orbital methods. XIX. Split-valence Gaussian-type basis sets for beryllium. *J. Chem. Phys.* **1977**, *66*, 879−880. (c) Hariharan, P. C.; Pople, J. A. The influence of polarization functions on molecular orbital hydrogenation energies. *Theor. Chim. Acta* **1973**, *28*, 213−222. (d) Hehre, W. J.; Pople, J. A. Self-Consistent Molecular Orbital Methods. XIII. An Extended Gaussian-Type Basis for Boron. *J. Chem. Phys.* **1972**, *56*, 4233−4234. (e) Hehre, W. J.; Ditchfield, R.; Pople, J. A. Self-Consistent Molecular Orbital Methods. XII. Further Extensions of Gaussian-Type Basis Sets for Use in Molecular Orbital Studies of Organic Molecules. *J. Chem. Phys.* **1972**, *56*, 2257−2261. (f) Ditchfield, R.; Hehre, W. J.; Pople, J. A. Self-Consistent Molecular-Orbital Methods. IX. An Extended Gaussian-Type Basis for Molecular-Orbital Studies of Organic Molecules. *J. Chem. Phys.* **1971**, *54*, 724−728.
(28) (a) Frisch, M. J.; Pople, J. A.; Binkley, J. S. Self-consistent molecular orbital methods 25. Supplementary functions for Gaussian basis sets. *J. Chem. Phys.* **1984**, *80*, 3265−3269. (b) Clark, T.;

Chandrasekhar, J.; Spitznagel, G. W.; Schleyer, P. V. R. Efficient diffuse function-augmented basis sets for anion calculations. III. The 3-21+G basis set for first-row elements, Li-F. *J. Comput. Chem.* **1983**, *4*, 294−301. (c) McLean, A. D.; Chandler, G. S. Contracted Gaussian basis sets for molecular calculations. I. Second row atoms, Z = 11−18. *J. Chem. Phys.* **1980**, *72*, 5639−5648. (d) Krishnan, R.; Binkley, J. S.; Seeger, R.; Pople, J. A. Self-consistent molecular orbital methods. XX. A basis set for correlated wave functions. *J. Chem. Phys.* **1980**, *72*, 650−654.

(29) (a) Marten, B.; Kim, K.; Cortis, C.; Friesner, R. A.; Murphy, R. B.; Ringnalda, M. N.; Sitkoff, D.; Honig, B. A New Model For Calculation of Solvation Free Energies: Correction of Self-Consistent Reaction Field Continuum Dielectric Theory for Short Range Hydrogen-Bonding Effects. *J. Phys. Chem.* **1996**, *100*, 11775−11788. (b) Tannor, D. J.; Marten, B.; Murphy, R.; Friesner, R. A.; Sitkoff, D.; Nicholls, A.; Honig, B.; Ringnalda, M.; Goddard, W. A. Accurate First Principles Calculation of Molecular Charge Distributions and Solvation Energies from Ab Initio Quantum Mechanics and Continuum Dielectric Theory. *J. Am. Chem. Soc.* **1994**, *116*, 11875−11882.

(30) It should be noted that the LC environment is different (i.e., more dense) from dichloromethane. Nonetheless, there is good correlation between the experimental and calculated results.

(31) (a) Jo, S.-Y.; Kim, B.-C.; Jeon, S.-W.; Bae, J.-H.; Walker, M.; Wilson, M.; Choi, S.-W.; Takezoe, H. Enhancement of the Helical Twisting Power with Increasing the Terminal Chain Length of Nonchiral Bent-Core Molecules Doped in a Chiral Nematic Liquid Crystal. *RSC Adv.* **2017**, *7*, 1932−1935. (b) Kim, B.-C.; Walker, M.; Jo, S.-Y.; Wilson, M. R.; Takezoe, H.; Choi, S.-W. Effect of Terminal Chain Length on the Helical Twisting Power in Achiral Bent-Core Molecules Doped in a Cholesteric Liquid Crystal. *RSC Adv.* **2018**, *8*, 1292−1295. (c) Ariga, K.; Mori, T.; Kitao, T.; Uemura, T. Supramolecular Chiral Nanoarchitectonics. *Adv. Mater.* **2020**, *32*, No. 1905657. (d) Mohammady, S.; Aldhayan, D.; Alshammri, M.; Alshammari, A.; Alazmi, M.; Katariya, K.; Jaremko, M.; Hagar, M. Polar Alkoxy Group and Pyridyl Effects on the Mesomorphic Behavior of New Non-Symmetrical Schiff Base Liquid Crystals. *Symmetry* **2021**, *13*, 1832.

(32) To save on computational time and resources we decided not to optimize the structures of model compounds **6** and **7**.

(33) Compounds **6**, **7**, and **12**−**15** resulted in a cholesteric to isotropic phase transition upon photoisomerization, and hence we were not able to collect their reflectance data. For more details, please see the SI.

(34) Kaspar, C.; Ravoo, B. J.; Van Der Wiel, W. G.; Wegner, S. V.; Pernice, W. H. P. The Rise of Intelligent Matter. *Nature* **2021**, *594*, 345−355.

https://doi.org/10.1021/jacs.4c07848
J. Am. Chem. Soc. 2024, 146, 24561−24569